International Journal of Nanomedicine

Dovepress
open access to scientific and medical research

Open Access Full Text Article

ORIGINAL RESEARCH

Resveratrol Loaded by Folate-Modified Liposomes Inhibits Osteosarcoma Growth and Lung Metastasis via Regulating JAK2/STAT3 Pathway

Wen Ting Zhu[1,*], Xiang Feng Zeng[2,*], Hua Yang[2], Meng Lei Jia[1], Wei Zhang[2], Wei Liu[2], Sheng Yao Liu[3]

[1]Department of Pharmacy, Biomedicine Research Center, Guangdong Provincial Key Laboratory of Major Obstetric Diseases, The Third Affiliated Hospital of Guangzhou Medical University, Guangzhou, 510150, People's Republic of China; [2]Department of Orthopedics, The Affiliated Nanhua Hospital, Hengyang Medical School, University of South China, Hengyang, 421001, People's Republic of China; [3]Department of Orthopedics, The Second Affiliated Hospital of Guangzhou Medical University, Guangzhou, 510260, People's Republic of China

*These authors contributed equally to this work

Correspondence: Wei Liu, Department of Orthopedics, The Affiliated Nanhua Hospital, Hengyang Medical School, University of South China, Hengyang, 421001, People's Republic of China, Email lwsurgery@163.com; Sheng Yao Liu, Department of Orthopedics, The Second Affiliated Hospital of Guangzhou Medical University, Guangzhou, 510260, People's Republic of China, Email liushengyao12@163.com

Background: Osteosarcoma is a malignant bone tumor with a high rate of lung metastasis and mortality. It has been demonstrated that resveratrol can inhibit tumor proliferation and metastasis, but its application is limited due to poor water solubility and low bioavailability. In this study, we proposed to prepare folate-modified liposomes loaded with resveratrol to investigate its anti-osteosarcoma effect in vitro and in vivo.

Methods: We prepared and characterized resveratrol liposomes modified with folate (denoted as, FA-Res/Lps). The effects of FA-Res /Lps on human osteosarcoma cell 143B proliferation, apoptosis, and migration were investigated by MTT, cell cloning, wound-healing assay, transwell, and flow cytometry. A xenograft tumor and lung metastasis model of osteosarcoma was constructed to study the therapeutic effects of FA-Res/Lps on the growth and metastasis of osteosarcoma in vivo.

Results: The FA-Res/Lps were prepared with a particle size of 118.5 ± 0.71 and a small dispersion coefficient of 0.154 ± 0.005. We found that FA-modified liposomes significantly increased resveratrol uptake by osteosarcoma cells 143B in flow cytometric assay, resulting in FA-Res/Lps, which inhibit tumor proliferation, migration and induce apoptosis more effectively than free Res and Res/Lps. The mechanism of action may be associated with the inhibition of JAK2/STAT3 signaling. In vivo imaging demonstrated that FA-modified DiR-modified liposomes significantly increased the distribution of drugs at the tumor site, leading to significant inhibition of osteosarcoma growth and metastasis by FA-Res/Lps. Furthermore, we found that FA-Res/Lps did not cause any adverse effects on mice body weight, liver, or kidney tissues.

Conclusion: Taken together, the anti-osteosarcoma effect of resveratrol is significantly enhanced when it is loaded into FA-modified liposomes. FA-Res/Lps is a promising strategy for the treatment of osteosarcoma.

Keywords: resveratrol, liposomes, osteosarcoma, lung metastasis, JAK2/STAT3 pathway

Introduction

Osteosarcoma (OS) is the most common malignant bone tumor. Most cases occur in children and young adults 10 to 30 years of age. Approximately 10 to 15% of patients with newly diagnosed osteosarcoma present with metastatic disease, primarily in the lung. The 5-year survival rate is approximately 60% among patients with localized osteosarcoma but is only 20% among patients presenting with metastases or recurrent disease.[1,2] The mainstay of treatment for OS is surgical resection of the primary tumor, pre-and post-operative chemotherapy has been effective in improving patient survival. Unfortunately, chemotherapeutic drugs are not good for treating OS lung metastases and are susceptible to toxic side effects, such as adriamycin, which has significant cardiac effects, so it is urgent to find a highly effective and less toxic

Received: 5 January 2023
Accepted: 14 April 2023
Published: 19 May 2023

drug for treating OS.[3,4] Nowadays, scientists are investigating the use of various naturally-occurring bioactive compounds against OS.[5,6]

Resveratrol (Res), a non-flavonoid polyphenolic organic compound, has antioxidant, anti-inflammatory,[7] anti-cancer,[8] and cardiovascular protection.[9] Furthermore, Res has a significant inhibitory effect on a wide range of tumor cells, including hepatocellular carcinoma,[10] breast cancer,[11] colon cancer,[12] gastric cancer[13], and leukemia.[14] Res has been demonstrated that it can inhibit the growth and metastasis of OS in vitro through NF-κB inhibition[15] and STAT3 pathway inhibition,[16] but there are few studies on the in vivo anti-tumor effects of Res, especially on the inhibition of OS metastasis. In addition, the preparation of injectable dosage forms of Res is hampered by its poor water solubility.[17,18]

The development of nano-delivery systems has addressed these issues, not only by improving the water solubility of drugs, but also by increasing their anti-tumor effects.[19] For example, liposome-encapsulated Res has been shown to improve the treatment of hepatocellular carcinoma[10] and glioblastoma,[18] and micelle-loaded Res and docetaxel have been shown to improve the treatment of drug-resistant tumors.[20] Although liposomes have several advantages such as low toxicity, biodegradability, biocompatibility, and enhanced permeability and retention (EPR) effect, their therapeutic effectiveness can be affected by inefficient drug delivery to the target cells.[21,22] Therefore, new systems of active targeting drug delivery have been introduced for the improvement of efficacy.[23] In this study, liposomes were selected as nanocarriers and also modified with folate (FA). Since the folate receptor is overexpressed on tumor cells,[24] we hypothesized that the folate-modified Res/Lps have good tumor targeting effects.

Herein, we constructed folate-modified liposome-loaded Res (denoted as, FA-Res/Lps), selected osteosarcoma 143B cells in vitro, a subcutaneous graft tumor in vivo, and a lung metastasis model with tail vein injection of 143B cells to examine the ability of FA-Res/Lps to inhibit tumor growth and lung metastasis and the possible mechanisms.

Materials and Method

Materials, Cell Culture, and Animals

Resveratrol was obtained from Macklin (Shanghai, China). DSPE-PEG_{2000}, FA-PEG_{2000}-DSPE was obtained from Ruixibio (Xi'an, China). Soy phosphatidylcholine, cholesterol, DiR iodide were purchased from Meilunbio (Dalian, China). Coumarin 6 (Cou-6) was obtained from Aladdin (Shanghai, China). JAK 2 antibody, P-STAT 3 antibody, Caspase 3 antibody, Cleaved Caspase 3 antibody were purchased from Cell Signaling Technology (Danvers, MA, USA). P-JAK 2 antibody was acquired from Abcam (Cambridge, UK). STAT 3 antibody, BCL-2 antibody, Bax antibody, Cytochrome antibody, and N Tubulin β polyclonal antibody were obtained from Bioworld Technology (Nanjing, China). The peroxidase-conjugated secondary antibody was obtained from CWBIO (Taizhou, China).

Human osteosarcoma cell line 143B cells were obtained from the Nanfang Hospital, Southern Medical University (Guangzhou, China). Cells were cultured in DMEM medium containing 10% FBS in a 37°C incubator containing 5% CO_2.

Male nude mice (6–8 weeks old) were purchased from Bestest (Zhuhai, China). All animal studies were conducted in accordance with the Guide for the Care and Use of Laboratory Animals. The Experimental Animal Ethics Committee of South China Hospital, South China University approved all experimental protocols.

Preparation and Characterization of the FA-Res/Lps

Resveratrol liposomes were prepared using the emulsification solvent volatilization method.[25] To prepare FA-Res/Lps, soy phosphatidylcholine, cholesterol, DSPE-PEG_{2000}, and FA-PEG_{2000}-DSPE (8.5:1:0.3:0.2 by mass) were dissolved in dichloromethane, respectively, and RES was dissolved in methanol. The mixture of lipid and Res was dripped into pure water under magnetic stirring at 450 rpm for 60 minutes. The resulting liposomal colostrum was sonicated 50 times using an ultrasonic cell crusher with an ultrasonic power of 200 W. The liposome solution is filtered through a 0.22 μm microporous membrane, freeze-dried before use and stored at room temperature. Coumarin 6 and DiR fluorescent liposomes were prepared in the same manner as the Res was replaced with coumarin 6 and DiR.

Intensity particle size and zeta potential were assessed using dynamic light scattering (DLS, Malvern, nano-ZS, UK). Res/Lps and FA-Res/Lps were stained with 2% phosphotungstic acid and their morphology was examined by

transmission electron microscopy (TEM, JEM-1400plus). The drug loading and encapsulation efficiency of Res/Lps and FA-Res/Lps were determined by UV spectrophotometry (SHIMADZU, UV −1780, Japan).

In vitro Cellular Uptake

143B cells were seeded in 6-well plates, the serum-free medium contained free Cou-6, Cou-6/Lps, and FA-Cou-6/Lps (the concentration of coumarin 6 was the same, 8ug/mL) were added for 2 h. The cells were collected after trypsin digestion and the intracellular fluorescence intensity of Cou-6 was detected by flow cytometry (Attune NxT, Thermo Fisher).

Cell Viability

143B cells were inoculated in 96-well plates at a density of 3×10^3 cells/well. Cells were then incubated with free Res, Res/Lps, and FA-Res/Lps, respectively. 48 hours later, incubation was altered with DMEM medium containing MTT (5 mg/mL) for 4 hours. MTT was then removed and 100 μL of DMSO was added dropwise to dissolve the methanogenic crystals at 37°C (dark, for 4 hours). Absorbance at 490 nm was measured using a microplate reader (Bio-Rad model 680, UK).

Colony Formation Unit Assay

143B cells were inoculated in six-well plates at a density of 1×10^3 cells/well. After cell attachment, cells were treated with free Res, Res/Lps, and FA-Res/Lps, respectively. Colonies were stained with crystal violet and photographed 7 to 10 days after administration.

Cell Apoptosis Analysis

Apoptosis was detected by flow cytometer through apoptosis assay kit (Beyotime, China). Cells were treated with free Res, Res/Lps, and FA-Res/Lps, respectively. After 48 hours of administration, cells were collected by centrifugation, washed twice with PBS, and resuspended in 200 μL Annexin V binding solution. Then, 5 μL Annexin V-FITC staining solution and 10 μL PI staining solution were added and the solutions were incubated in the dark for 15 minutes and immediately tested by flow cytometry.

Transwell Migration Assay

Cell migration experiments were performed using transwell chambers with a pore size of 8μm. The density of the cell suspension was 1.5×10^6 cells/mL, serum-free medium was added to the upper chamber of the transwell and 10% FBS medium was added to the lower chamber. At the same time, drugs were added to the upper chamber and treated with free Res, Res/Lps, and FA-Res/Lps, individually. After 24 hours of treatment, the non-migrating cells in the upper chamber were wiped with a cotton swab, fixed with 4% formaldehyde and stained with crystalline violet, and photographed.

Wound-Healing Assay

The 143B cells were inoculated into 6-well plates in a 37°C, 5% CO_2 incubator. When the cells reached 100% confluence, three parallel lines were drawn evenly at the bottom of each well with a 200 μL needle tip. Cells were treated with 10% fetal bovine serum medium containing free Res, Res/Lps, and FA-Res/Lps, separately. Finally, photographs were taken and the width of the scratch was measured at 0 h and 24 h, respectively.

Western Blot Analysis

The 143B cells were inoculated in cell culture dishes and divided into 4 groups and treated with free Res, Res/Lps, and FA-Res/Lps. Cells were extracted from protein by RIPA lysis buffer containing a mixture of protease and phosphatase inhibitors and protein concentrations were measured using the BCA method. Use SDS-PAGE gels for protein separation. Protein samples were transferred to PVDF membranes, closed with 5% skimmed milk (Solarbio, Beijing), washed twice with TBST and then treated with appropriately diluted primary antibodies (p-JAK2, diluted 1:1000; JAK2, diluted 1:1000; p-STAT3, diluted 1:1000; STAT3, diluted 1:1000; BCL-2. diluted 1:1000; Bax, diluted 1:1000; Caspase3, diluted

1:1000; Cleaved Caspase3, diluted 1:1000; Cytochrome, diluted 1:1000; N-Cadherin, diluted 1:1000; Vimentin, diluted 1:1000; Tubulin, diluted 1:1000) overnight at 4°C. After washing three times with TBST, samples were incubated with secondary antibodies for 1 h at room temperature and developed using ECL illumination solution (Millipore, USA).

In vivo Imaging

In vivo biodistribution of drugs was performed. Osteosarcoma 143B cells were grafted subcutaneously to nude mice, and when the volume grew to about 350 mm^3, free DiR, DiR liposomes, and FA-DiR liposomes were injected into nude mice via the tail vein. The concentration of DiR was 0.5 mg/kg and the biodistribution of DiR in vivo was investigated by a Xenogen IVIS100 imaging system (XenogenCorp. Hopkinton, MA, USA). Mice were executed at 24 hours and the fluorescence intensity of major organs (heart, liver, spleen, kidney, and tumor) was measured.

In vivo Antitumor Effects

Approximately 100 μL of 7×10^6 143B cells in DMEM were mixed with 100 μL of matrigel gel (Corning, USA) and implanted subcutaneously into the backs of mice. Mice were randomly divided into 4 groups (n=3) at tumor volume of 100 mm^3 (approximately 1 week after injection) and injected intraperitoneally with saline, Res (10 mg/kg), Res/Lps (10 mg/kg), and FA-Res/Lps (10 mg/kg) every 2 days. Next, tumor size was measured every 3 days using vernier calipers, tumor volume (V) = length*$width^2$/2. Antitumor efficacy was determined based on tumor growth and final tumor weight.

In Vivo Anti-Lung Metastatic Effects

Stably transfected 143B cells expressing luciferase (143B-luc; 1 x 10^6 Cells/Mice) were injected into mice via the tail vein.[26,27] The development of lung metastases were assessed using the in vivo imaging system (IVIS, XenogenCorp. Hopkinton, MA, USA). Three days after injection, mice were randomly divided into four groups (n=5) and injected intraperitoneally with saline, Res (10 mg/kg), Res/Lps (10 mg/kg), and FA-Res/Lps (10 mg/kg) every two days. Mice were tracked for body weight and executed 4 weeks after administration. Lung tissue was extracted and luminescence intensity was taken.

Hematoxylin and Eosin (H&E) Staining

After execution of the mice, liver, spleen, kidney, lung, and tumor tissue were embedded in paraffin. The sections were dewaxed, stained with hematoxylin nuclear staining concentrate and 0.5% eosin staining solution, and sealed with neutral glue. These photographs were detected in five random fields using a microscope (Nikon, Ni-u, Tokyo, Japan).

Immunohistochemistry (IHC) Staining

Paraffin sections were dewaxed in xylene and then rehydrated in an alcohol gradient. Tissue antigen was then heated in sodium citrate at pH 6.0 for 15 minutes, sections were closed with serum and incubated with anti-ki67 primary antibody (diluted 1:100) overnight at 4°C. After three rinses in PBS, sections were incubated with secondary antibody for 10 minutes at room temperature. Then, 1–2 drops of DABPlus developer were mixed with 1 mL of DAB plus substrate and incubated with the sections for 5 ~ 15 minutes. Samples were examined under a microscope (Nikon, Ni-u, Tokyo, Japan) and ki-67 positive cells were counted in 5 random fields.

TUNEL Assay

Apoptotic cells were studied in vivo by TdT-mediated dUTP nick end labeling (TUNEL, KeyGEN BioTECH, Jiangsu). First, paraffin sections were dehydrated and transparent, then permeabilized with DNase-free proteinase K and then washed three times with PBS. The prepared TUNEL assay solution was added to the sections and incubated at 37°C for 60 minutes. Finally, sections were mounted with an anti-fluorescence burst mounting solution and observed under a confocal microscope (Nikon, A1R+N-STORM, Tokyo, Japan).

Statistical Analysis

Images were drawn using GraphPad Prism 9 (GraphPad Software, San Diego, CA, USA). SPSS 17.0 was used for statistical analysis. One-way analysis of variance (ANOVA) was used to analyze the significance between groups. All data are expressed as mean ± SD, with $P<0.05$ indicating significance.

Results

The Characterization of FA-Res/Lps

The appearance of Res/Lps and FA-Res/Lps is shown in Figure 1A, where clarified solutions of Res/Lps and FA-Res/Lps were observed, indicating that liposome delivery of Res optimizes solubility issues. In addition, Res/Lps and FA-Res/Lps can be lyophilized into powder form. TEM results show that both Res/Lps and FA-Res/Lps have a spherical shape (Figure 1B and C). As shown in Figure 1D and E, the particle sizes of Res/Lps and FA-Res/Lps were 100.3 ± 0.35 nm and 118.5 ± 0.71 nm, respectively, and the polymer dispersion index (PDI) was 0.172 ± 0.025 and 0.154 ± 0.005, respectively. Furthermore, the zeta potentials of Res/Lps and FA-Res/Lps were −32.8 ± 0.14 mV and −33.0±0.81 mV. The encapsulation efficiencies of Res/Lps and FA-Res/Lps were 93 ± 2.4% and 91 ± 1.3%, respectively (Figure 1F and

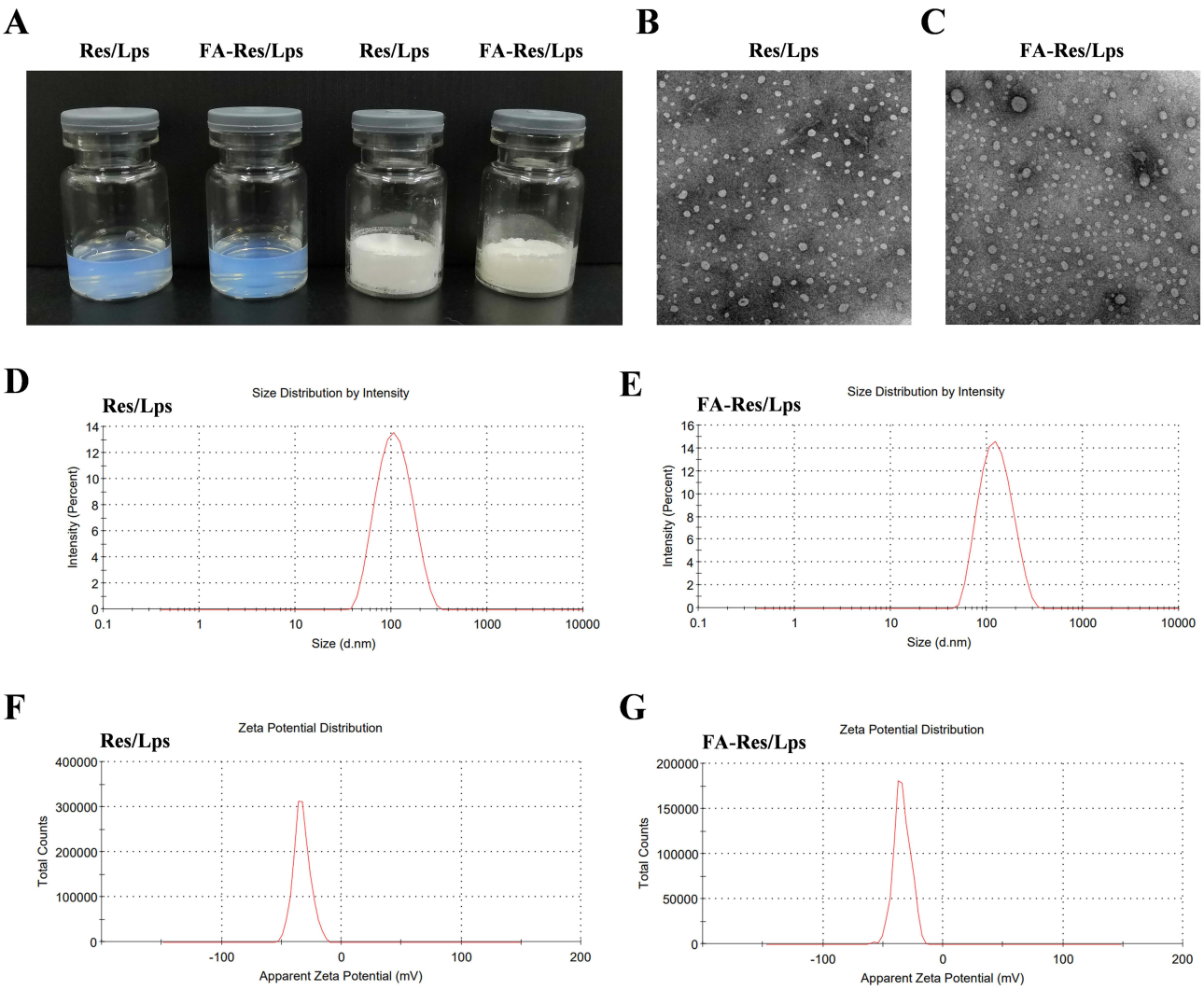

Figure 1 Characterization of FA-Res liposomes. (**A**) Photographs of Res liposomes and FA-Res liposomes. (**B** and **C**) The TEM images of Res liposomes and FA-Res liposomes. (**D** and **E**) Particle size distribution of Res liposomes and FA-Res liposomes. (**F** and **G**) Zeta potential of Res liposomes and FA-Res liposomes.

G). Also, the particle size and encapsulation rate of the redissolved Res/Lps and FA-Res/Lps were consistent with those before lyophilization.

FA-Res/Lps Inhibits Proliferation and Induces Apoptosis of Osteosarcoma Cells

We used flow cytometry to assay the cellular uptake of free Cou-6, Cou-6/Lps and different proportions of FA-PEG_{2000}-DSPE modified Cou-6 Liposomes in 143B cells (Figure 2A). We found that 2% FA-PEG_{2000}-DSPE modified Cou-6 liposomes had the highest cumulative Cou-6 concentration. Therefore, we chose 2% FA as the modification ratio of FA-Res/Lps.

Next, we assessed the cytotoxicity of free Res, Res/Lps, and FA-Res/Lps in 143B cells. Notely, FA-Res/Lps significantly increased the cytotoxicity of 143B cells (Figure 2B). To further confirm the effect of FA-Res/Lps on the proliferation of 143B cells, we performed cell clone formation (Figure 2C). The number of clones in the control, free Res, Res/Lps, and FA-Res/Lps groups were 284.7 ± 10, 225 ± 9.2 ($P < 0.05$, compared to control), 141.7 ± 6.2 ($P < 0.01$, compared to control) and 14.6 ± 1.3 ($P < 0.01$, compared to Res/Lps), respectively (Figure 2D).

Annexin V-FITC/PI double staining was used to detect apoptosis in 143B cells (Figure 2E). The apoptosis rates in 143B cells were 7.1±2.1%, 20.6±1.8% ($P<0.01$, compared with control) and 30.9±1.2% ($P<0.01$, compared with control) in the control, free Res and Res/Lps groups, respectively, while the FA-Res/Lps group significantly increased the apoptosis rate to 51.1±2.6% ($P<0.01$, compared with Res/Lps) (Figure 2F). In addition, the expression of the corresponding apoptotic proteins Bax/Bcl-2 ratio, cytochrome C, and cleaved caspase-3 was significantly upregulated in the FA-Res /Lps group (Figure 2G).

FA-Res/Lps Inhibits Osteosarcoma Cell Invasion and Migration

The effect of FA-Res/Lps on the migration of osteosarcoma cells was examined using the transwell assay and the wound healing assay. In Figure 3A, the free Res and Res/Lps treatments successfully blocked the migration of OS cells through the pores into the inferior chamber compared to the control group ($p<0.01$, compared to the control group). However, the FA-Res/Lps group further reduced the entry of cells into the lower chamber compared to the free Res and Res/Lps groups ($p<0.05$, compared to Res/Lps) (Figure 3B). This phenomenon also occurred in the wound healing assay (Figure 3C), 24 hours after treatment of 143B cells with Res, the wound healing rates in the control, free Res and Res/Lps groups were 79.4±1.1%, 59.9±2.3% ($p<0.01$, compared to control) and 41±0.8% ($p<0.0001$, compared to control), respectively, whereas the FA- Res/Lps treatment group had a stronger inhibitory effect on wound healing than the free Res and Res/Lps groups, with a wound healing rate of 29.3±1.8% ($p<0.05$, compared with Res/Lps) (Figure 3D).

To further explore the mechanism of reduced cell migration, protein levels of metastasis-related proteins, such as N-cadherin and Vimentin, were measured by western blot in cells from the control, free Res, Res/Lps, and FA-Res/Lps groups. The results showed that FA-Res/Lps significantly decreased the expression of metastasis-related proteins (Figure 3E). The JAK2/STAT3 signaling pathway, as a major chain of intracellular signaling, plays an important role in cell proliferation, apoptosis, invasion, migration, and immune response activities. Western blot results showed that FA-Res/Lps significantly decreased the expression of P-JAK2 and P-STAT3 protein expression (Figure 3F).

In vivo Biodistribution of FA-DiR/Lps

The distribution of DiR liposomes in nude mice was examined by an in vivo imaging system. Identical doses of free DiR, DiR liposomes, and FA-DiR/Lps were injected into mice via the tail vein. The in vivo DiR distribution was examined 24 hours after administration (Figure 4A), and the fluorescence intensity of free DiR, DiR liposomes, and FA-DiR liposomes was $(1.5±0.3)x10^{10}$, $(13.9±2.2)x10^{10}$ ($P<0.05$, compared with the free DiR group) and $(19.5±1.7)x10^{10}$ ($P<0.05$, compared with the DiR liposome group for comparison) in vivo tumor tissues (Figure 4B). This indicates that folate-modified liposomes prolong liposome circulation and target tumors in vivo. Figure 4C shows fluorescence images of major organs and tumors 24 hours after injection, the fluorescence intensity of isolated tumor tissues was $(6.7±1.6)x10^{9}$, $(57.8±7.7)x10^{9}$, $(88.8±4.6)x10^{9}$ for free DiR, DiR liposomes and FA-DiR liposomes ($P<0.05$, compared to the DiR liposome group) (Figure 4D), which further indicated that FA-DiR liposomes exhibited high tumor accumulation.

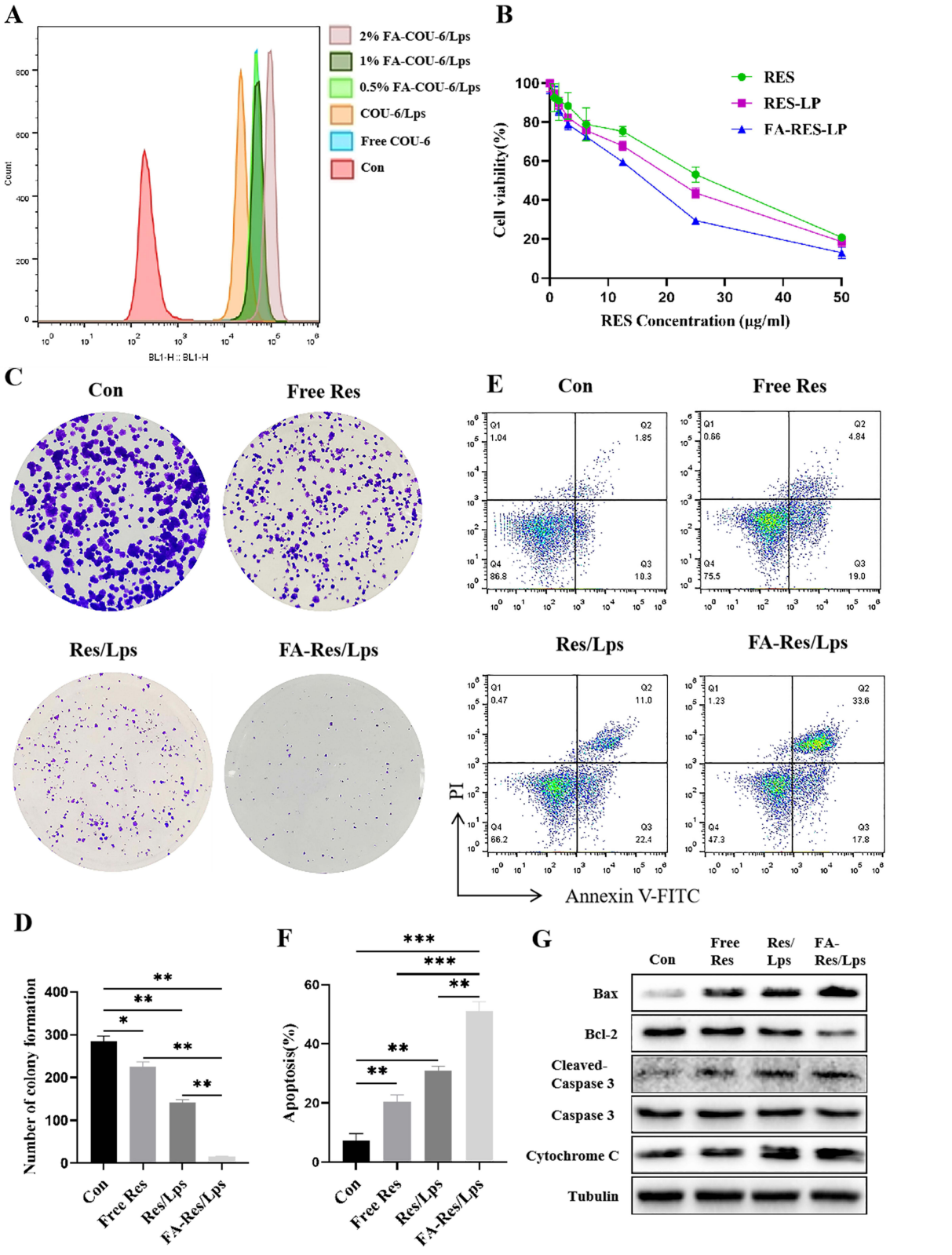

Figure 2 Proliferation and apoptosis of FA-Res liposome-treated osteosarcoma cells and their associated signaling pathways. (**A**) Cellular uptake of free COU-6, COU-6 liposomes, and FA-COU-6 liposomes by 143B cells. (**B**) Cell viability of 143B cells after 48 h treatment with free Res, Res liposomes, and FA-Res liposomes. (**C** and **D**) The clonogenic capacity of 143B cells and their colony number were calculated. (**E** and **F**) Apoptosis analysis of 143B cells by double staining with FITC Annexin V/PI and the percentage of apoptosis was calculated. (**G**) Expression of Bax, Bcl-2, Caspase-3, Cleaved Caspase-3, and cytochrome C proteins in 143B cells was detected by western blot analysis. All data are expressed as mean ± SD (n=3). *p<0.05, **p<0.01 and ***p<0.001.

https://doi.org/10.2147/IJN.S398046 DovePress

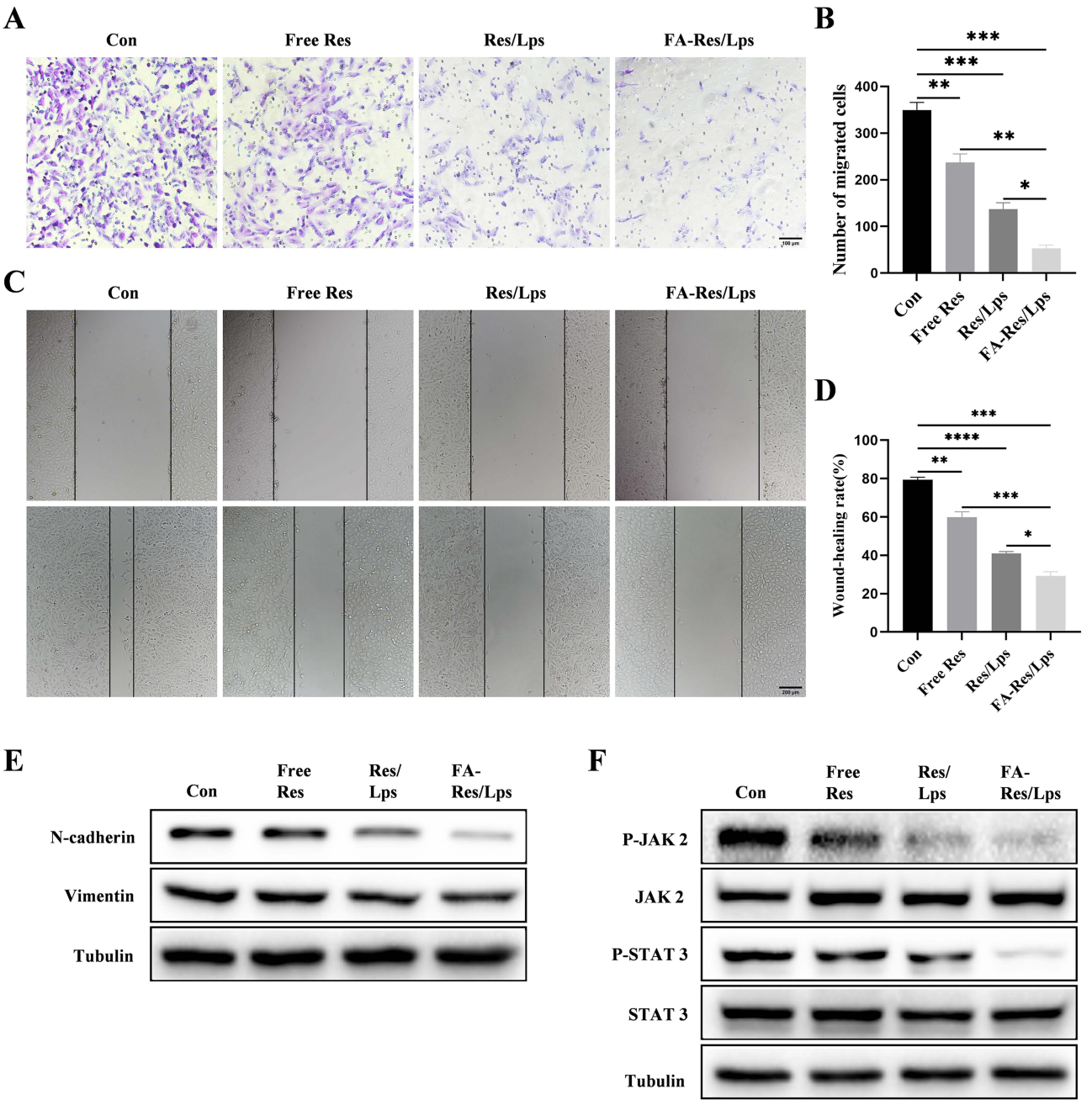

Figure 3 Cell migration and associated signalling pathways in FA-Res liposome-treated osteosarcoma cells. (**A** and **B**) Representative images and quantitative data of transwell analysis of 143B cells after 24 hours of treatment with control, free Res, Res liposomes, and FA-Res liposomes, respectively. (**C** and **D**) Wound healing of 143B cells after 0 h and 24 h of treatment with control, free Res, Res liposomes, and FA-Res liposomes, respectively, was photographed and their relative healing rates were calculated. (**E**) Expression of N-Cadherin and vimentin protein in 143B cells were analyzed by Western blot. (**F**) Expression of P-JAK 2, JAK 2, P-STAT 3, and STAT 3 proteins in 143B cells were analyzed by western blot. All data are expressed as mean ± SD (n=3). *p<0.05, **p<0.01, ***p<0.001, ****p<0.0001.

FA-Res/Lps Suppresses Tumor Growth in vivo

We investigated the antitumor effect of FA-Res/Lps on 143B cell xenograft mice. Figure 5A shows photographs of mice from each group, the tumor volumes in the control, free Res, Res/Lps, and FA-Res/Lps groups were 1239.3±123.5 mm^3, 995.4±53.6 mm^3 (P<0.05, compared with the control group), 601.7±43.3 mm^3 (P<0.0001, compared with the control group), and 433.4±69.3 mm^3 (P<0.0001, compared with the control group) (Figure 5B and C). The tumor weights were 0.94±0.09 g, 0.69±0.05 g (P<0.05, compared with the control group), 0.45±0.04 g (P<0.01, compared with the control group), and 0.26±0.07 g (P<0.001, compared with the control group), respectively (Figure 5D). More importantly, we

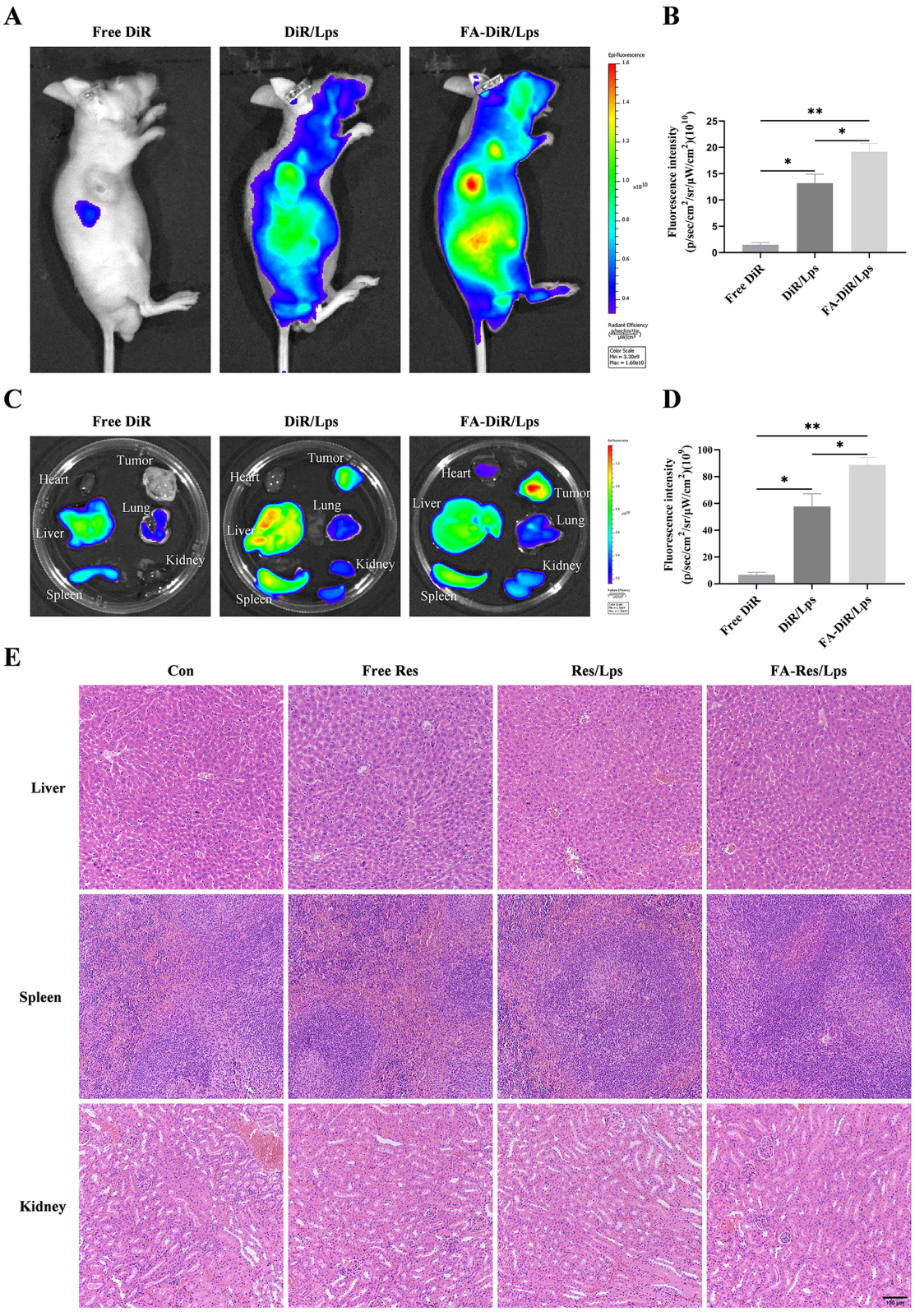

Figure 4 Biodistribution of FA-DiR liposome treatment in 143B xenograft mice. (**A** and **B**) Representative in vivo fluorescence images and quantification of fluorescence intensity of DiR-loaded liposomes in 143B cell-induced xenograft mice. (**C** and **D**) Representative fluorescence images and quantification of fluorescence intensity of organs and tumors in mice 24 hours after DiR injection. (**E**) Representative HE-stained images of liver, spleen, and kidney tissues from each group of transplanted tumor model mice. All data are expressed as mean ± standard deviation (n=3). *p<0.05, **p<0.01.

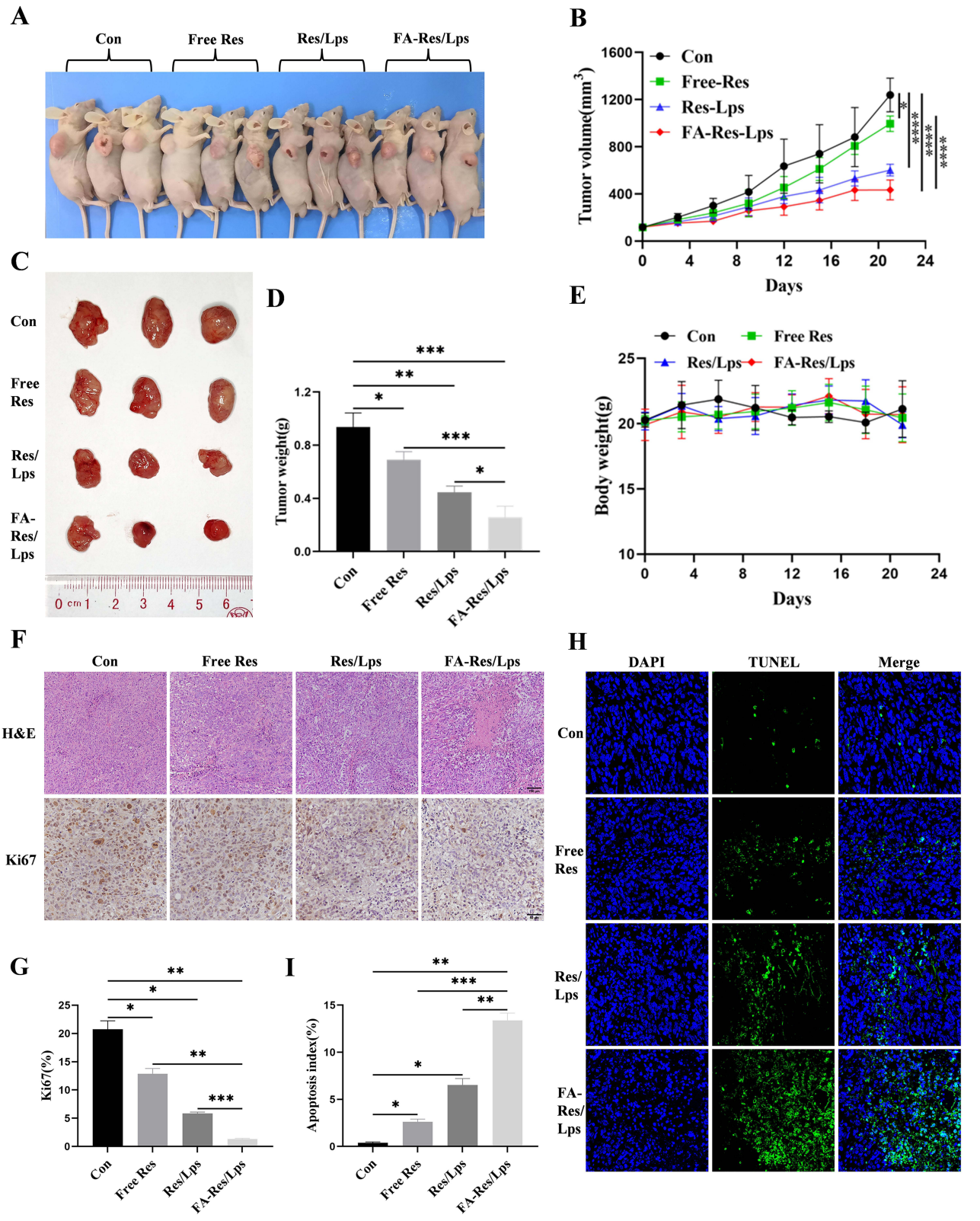

Figure 5 Antitumor effect of FA-Res liposomes treatment in 143B xenograft mice. (**A**) Representative in vivo animal photographs of 143B-induced xenograft tumor-bearing mice. (**B**) Curves of changes in subcutaneous tumor volume in each group. (**C**) Photographs of each group of subcutaneous tumors. (**D**) Weight of each group of subcutaneous tumors. (**E**) Body weights of transplanted tumor-bearing mice treated with control, free Res, Res liposomes, and FA-Res liposomes, respectively. (**F**) Representative HE staining images and Ki67 immunohistochemistry images of each group of tumors. (**G**) Quantitative Ki67 immunohistochemistry data for each group of tumors. (**H** and **I**) Representative TUNEL staining images and quantitative TUNEL staining data for each group of tumors. All data are expressed as mean ± standard deviation (n=3). *p<0.05, **p<0.01, ***p<0.001, ****p<0.0001.

noted no significant changes in body weight or organ morphology in mice after FA-Res/Lps treatment (Figure 4E and 5E). These results suggest that FA-Res/Lps enhance the anti-osteosarcoma effects without causing major organ-related toxicity.

The HE staining of tumor tissues (Figure 5F) showed that the FA-Res/Lps treatment group had significantly more foci of necrosis and fibrosis than the other groups. In addition, the anti-proliferation marker Ki67 (Figure 5F) showed that FA-Res/Lps reduced the expression of proliferation markers in tumor cells ($p<0.001$, compared to the control group) (Figure 5G). Based on the above findings, FA-Res/Lps inhibit tumor growth in vivo by suppressing cell proliferation.

In addition, the TUNEL assay was used to detect apoptosis in vivo. As shown in Figure 5H, green fluorescence was observed in osteosarcoma tumor tissues from the drug-treated group. The apoptotic index was significantly higher in the FA-Res/Lps group (13.39 ± 0.62%, $P<0.01$, compared to the control group) than in the group treated with free Res (2.61 ± 0.25%, $P<0.001$, compared to the FA-Res/Lps group) and Res liposomes (6.52% ± 0.56%, $P<0.01$, compared with the FA-Res/Lps group) (Figure 5I) treated groups. These results suggest that induction of apoptosis in tumor cells is another anti-tumor mechanism in vivo.

FA-Res/Lps Inhibits Lung Metastasis of Osteosarcoma in vivo

To assess whether FA-Res/Lps inhibit the lung metastases of osteosarcoma, we monitored the lung luminescence intensity in mice by in vivo imaging system. As shown in Figure 6A and B, free Res and Res/Lps-treated mice had lower lung luminescence intensity than controls ($P<0.05$, compared to controls), but they had higher lung luminescence intensity than the FA-Res/Lps group ($P<0.05$, compared to the FA-Res/Lps group). We executed the mice and obtained lung tissues, and the luminescence intensity of isolated lung tissues obtained by the IVIS method was consistent with the in vivo results ($P<0.01$) (Figure 6C and D).

Also, there were fewer and smaller pulmonary metastases on the lung surface in the FA-Res/Lps-treated group compared to the free Res and Res/Lps-treated groups. The biopsy results were also confirmed by HE staining of lung tissues (Figure 6E and F), with the number of lung nodules in the control, free Res, Res/Lps, and FA-Res/Lps groups being 26.7±2.1, 19.0±1.6 ($P<0.05$ compared to control), 11.3±1.7 and 4.3±0.9 ($P<0.05$ compared to Res/Lps), respectively. In addition, we noted no significant changes in the body weight of mice after FA-Res/Lps treatment (Figure 6G). This suggests that FA-Res/Lps are safe and non-toxic.

Discussion

In this study, FA-Res/Lps was found to significantly induce apoptosis and inhibit cell proliferation, migration in osteosarcoma cells, and its effect was superior to that of free Res and Res/Lps. The folate-modified liposomes had a good tumor-targeting effect and effectively inhibited tumor growth and lung metastasis *in* vivo.

Liposomes are biocompatible nanocarriers and liposomal nanomedicines on the market that show good promise for clinical applications.[28,29] Many herbal monomers achieve improved water solubility and enhanced bioavailability through liposomal drugs. For example, oridonin-loaded long-circulating liposomes showed good anti-colon cancer activity.[30] The small size (<200 nm) nanoparticles have a propensity to evade scavenging by the reticuloendothelial system (RES) and passively targeting solid tumors through the EPR effect.[21,31] Nevertheless, passive targeting of nanodrugs is less effective because of insufficient accumulation of nanoparticles in the tumor and poor pharmacokinetics.[32] More specifically, modification of folate,[33] transferrin[18], and cell-penetrating peptides[34] on the surface of liposomes can enhance their active targeting effect and further improve the anti-tumor effect of the drugs.[23] Recently, folate has gained much attention as a targeted drug delivery agent due to its small size, high in vivo stability, low immunogenicity, and high binding affinity with folate receptors (FRs).[35] The FRs are overexpressed in tumors, while only minimally distributed in normal tissues.[24] Liposomes, dendrimers, and other nanoparticles decorated with folate molecules can be internalized by FRs.[24] This study developed FA modification liposomes to enhance Res retention in tumors as well as facilitate their cellular uptake by FR-mediated endocytosis,[36] allowing Res to more precisely and effectively target OS. Take together, the superior anticancer efficacy of FA-Res/Lps is associated with its smaller particle size, higher drug encapsulation efficiency, and active targeting, which is consistent with the findings of Shirleide Santos

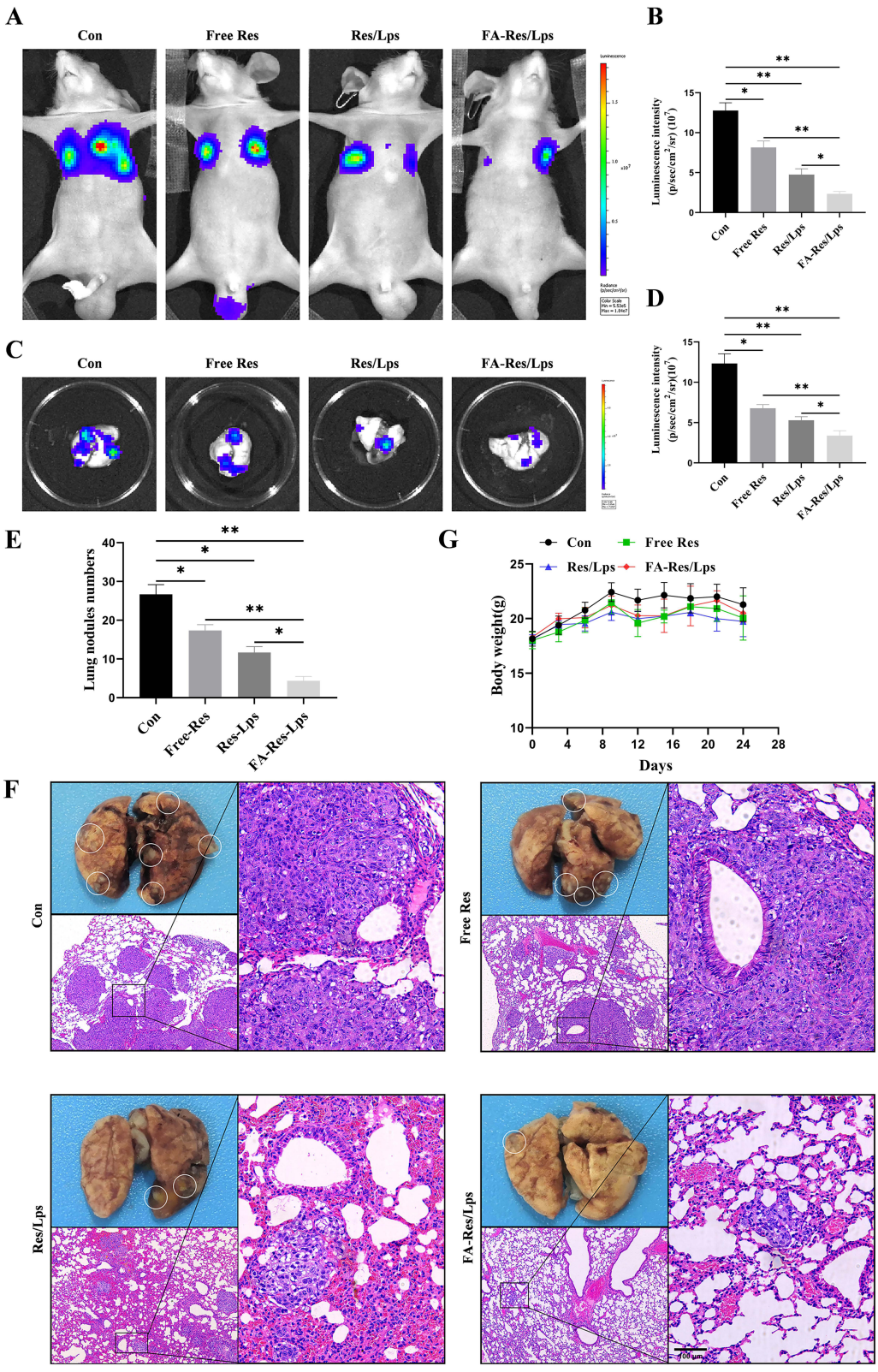

Figure 6 FA-Res liposomes inhibited the lung metastases of osteosarcoma in vivo. (**A**–**D**) Fluorescence imaging of luciferase and quantitative data in OS lung metastases mouse model in vivo, and lung tissues ex vivo at 4 weeks. (**E**) Number of lung nodules in mice in each treatment group. (**F**) Representative photographs of lung tissues of mice in each group and representative HE-stained images of lung tissues. (**G**) Changes in body weight of mice in each treatment group. All data are expressed as mean ± standard deviation (n=5). *p<0.05, **p<0.01.

Nunes,[33] where the folate-coated pH-sensitive formulation had significantly better antitumor activity than the pH-dependent system only or the free drug.

FA-Res/Lps modified with folate increased the intracellular concentration of the drug, and we found that it was more effective in inhibiting tumor cell proliferation and inducing apoptosis. The JAK2/STAT3 signaling pathway, plays an important role in cell proliferation, apoptosis, invasion, migration, and immune response activities.[37,38] Triggered by cytokines and interferons, this pathway rapidly transduces extracellular signals into the nucleus and is aberrantly expressed in a variety of tumors including head and neck squamous cell carcinoma, lung, oesophageal, gastric, liver, colorectal, and myeloproliferative neoplasms.[38,39] Our results showed that FA-Res/Lps inhibited the expression of p-JAK2 and p-STAT3 proteins, thereby inducing apoptosis. In vivo, Ki67 staining confirmed that FA-Res/Lps could inhibit tumor cell proliferation, and TUNEL staining demonstrated that FA-Res/Lps could exert anti-tumor effects by inducing apoptosis in tumor cells.

The main cause of death in OS is lung metastasis, and it has been documented that Res effectively inhibits the invasion and migration of OS cells.[40] The present study builds on previous studies and further demonstrates that Res loaded by folate-modified liposomes effectively enhances its ability to inhibit cell invasion and migration in vitro compared to free Res and Res/Lps. In addition, we also constructed a lung metastasis model by tail vein injection of 143B-luc cells, and the results showed that FA-Res/Lps significantly inhibited OS lung metastasis. In the future, we may be able to develop orthotopic tumor and lung metastasis mouse models of OS to study the effects of drugs on tumor growth and metastasis.[41,42]

Finally, we also clarified that folate-modified liposomal delivery of Res did not increase toxicity to mice by examining body weight, liver, and kidney HE staining. Moreover, Res can enhance the sensitivity of cancer cells to doxorubicin[43] and cisplatin[44] and ameliorate their adverse impact on normal cells and organs, such as the liver, kidney, and brain.[45] Overall, FA-Res/Lps has good safety and efficacy in the pre-clinical treatment of OS. Simultaneously, since the folate receptor is aberrantly expressed in numerous malignancies including breast, colon, lung, and kidney cancer,[35,36] the proposed FA-Res /Lps may be applied to a wide variety of tumors.

Conclusion

Resveratrol loaded by folate-modified liposomes could effectively enhance its uptake by tumor cells and increase its enrichment at tumor sites in vivo. This makes FA-Res/Lps significantly more effective than free Res and Res/Lps in inhibiting osteosarcoma proliferation and metastasis in vitro and in vivo, probably through inhibition of the JAK2/STAT3 signaling pathway. The efficacy and safety of FA-Res/Lps could provide a new strategy for osteosarcoma treatment.

Acknowledgments

This work was supported by Hunan Provincial Natural Science Foundation of China (2022JJ30546), the clinical medical technology innovation guided program of Hunan Province Science and Technology Department (2020SK51902), Guangzhou Science and Technology Plan Project (202102020149, 202102020536), Academician He Lin Scientific Research Fund (2021HLKY07), Scientific research project of Traditional Chinese Medicine Bureau of Guangdong Province (20221248) and University of South China Innovation Foundation For Postgraduate (223YXC034).

Disclosure

The authors declare no conflicts of interests.

References

1. Gianferante DM, Mirabello L, Savage SA. Germline and somatic genetics of osteosarcoma - connecting aetiology, biology and therapy. *Nat Rev Endocrinol*. 2017;13(8):480–491. doi:10.1038/nrendo.2017.16
2. Yang C, Tian Y, Zhao F, et al. Bone microenvironment and osteosarcoma metastasis. *Int J Mol Sci*. 2020;21(19). doi:10.3390/ijms21196985
3. Jiang ZY, Liu JB, Wang XF, Ma YS, Fu D. Current status and prospects of clinical treatment of osteosarcoma. *Technol Cancer Res T*. 2022;21:15330338221124696. doi:10.1177/15330338221124696
4. Benjamin RS. Adjuvant and neoadjuvant chemotherapy for osteosarcoma: a historical perspective. *Adv Exp Med Biol*. 2020;1257:1–10. doi:10.1007/978-3-030-43032-0_1

5. Tobeiha M, Rajabi A, Raisi A, et al. Potential of natural products in osteosarcoma treatment: focus on molecular mechanisms. *Biomed Pharmacother*. 2021;144:112257. doi:10.1016/j.biopha.2021.112257
6. Wang T, Zhang C, Wang S. Ginsenoside Rg3 inhibits osteosarcoma progression by reducing circ_0003074 expression in a miR-516b-5p/KPNA4-dependent manner. *J Orthop Surg Res*. 2021;16(1):724. doi:10.1186/s13018-021-02868-7
7. Grinan-Ferre C, Bellver-Sanchis A, Izquierdo V, et al. The pleiotropic neuroprotective effects of resveratrol in cognitive decline and Alzheimer's disease pathology: from antioxidant to epigenetic therapy. *Ageing Res Rev*. 2021;67:1.
8. Ren B, Kwah MX, Liu C, et al. Resveratrol for cancer therapy: challenges and future perspectives. *Cancer Lett*. 2021;515:63–72. doi:10.1016/j.canlet.2021.05.001
9. Cheng CK, Luo JY, Lau CW, Chen ZY, Tian XY, Huang Y. Pharmacological basis and new insights of resveratrol action in the cardiovascular system. *Brit J Pharmacol*. 2020;177(6):1258–1277. doi:10.1111/bph.14801
10. Jagwani S, Jalalpure S, Dhamecha D, Jadhav K, Bohara R. Pharmacokinetic and pharmacodynamic evaluation of resveratrol loaded cationic liposomes for targeting hepatocellular carcinoma. *Acs Biomater Sci Eng*. 2020;6(9):4969–4984. doi:10.1021/acsbiomaterials.0c00429
11. Wu H, Chen L, Zhu F, Han X, Sun L, Chen K. The cytotoxicity effect of resveratrol: cell cycle arrest and induced apoptosis of breast cancer 4T1 cells. *Toxins*. 2019;11(12):731. doi:10.3390/toxins11120731
12. Yuan L, Zhou M, Huang D, et al. Resveratrol inhibits the invasion and metastasis of colon cancer through reversal of epithelial- mesenchymal transition via the AKT/GSK-3beta/Snail signaling pathway. *Mol Med Rep*. 2019;20(3):2783–2795. doi:10.3892/mmr.2019.10528
13. Lin M, Yao W, Xiao Y, et al. Resveratrol-modified mesoporous silica nanoparticle for tumor-targeted therapy of gastric cancer. *Bioengineered*. 2021;12(1):6343–6353. doi:10.1080/21655979.2021.1971507
14. Huang XT, Li X, Xie ML, et al. Resveratrol: review on its discovery, anti-leukemia effects and pharmacokinetics. *Chem-Biol Interact*. 2019;306:29–38. doi:10.1016/j.cbi.2019.04.001
15. Xu N, Wang L, Fu S, Jiang B. Resveratrol is cytotoxic and acts synergistically with NF-kappaB inhibition in osteosarcoma MG-63 cells. *Arch Med Sci*. 2021;17(1):166–176. doi:10.5114/aoms.2020.100777
16. Peng L, Jiang D. Resveratrol eliminates cancer stem cells of osteosarcoma by STAT3 pathway inhibition. *PLoS One*. 2018;13(10):e0205918. doi:10.1371/journal.pone.0205918
17. Walle T, Hsieh F, DeLegge MH, Oatis JJ, Walle UK. High absorption but very low bioavailability of oral resveratrol in humans. *Drug Metab Dispos*. 2004;32(12):1377–1382. doi:10.1124/dmd.104.000885
18. Jhaveri A, Deshpande P, Pattni B, Torchilin V. Transferrin-targeted, resveratrol-loaded liposomes for the treatment of glioblastoma. *J Control Release*. 2018;277:89–101. doi:10.1016/j.jconrel.2018.03.006
19. Liu Y, Li Q, Bai Q, Jiang W. Advances of smart nano-drug delivery systems in osteosarcoma treatment. *J Mater Chem B*. 2021;9(27):5439–5450. doi:10.1039/d1tb00566a
20. Guo X, Zhao Z, Chen D, et al. Co-delivery of resveratrol and docetaxel via polymeric micelles to improve the treatment of drug-resistant tumors. *Asian J Pharm Sci*. 2019;14(1):78–85. doi:10.1016/j.ajps.2018.03.002
21. de Lazaro I, Mooney DJ. A nanoparticle's pathway into tumors. *Nat Mater*. 2020;19(5):486–487. doi:10.1038/s41563-020-0669-9
22. Abri AM, Bagheri R, Mosafer J, et al. Recent advances on thermosensitive and pH-sensitive liposomes employed in controlled release. *J Control Release*. 2019;315:1–22. doi:10.1016/j.jconrel.2019.09.018
23. Pandit S, Dutta D, Nie S. Active transcytosis and new opportunities for cancer nanomedicine. *Nat Mater*. 2020;19(5):478–480. doi:10.1038/s41563-020-0672-1
24. Farran B, Montenegro RC, Kasa P, et al. Folate-conjugated nanovehicles: strategies for cancer therapy. *Mat Sci Eng C-Mater*. 2020;107:1.
25. Chen YQ, Zhu WT, Lin CY, Yuan ZW, Li ZH, Yan PK. Delivery of rapamycin by liposomes synergistically enhances the chemotherapy effect of 5-fluorouracil on colorectal cancer. *Int J Nanomed*. 2021;16:269–281. doi:10.2147/IJN.S270939
26. Zhang Y, Liu Z, Yang X, et al. H3K27 acetylation activated-COL6A1 promotes osteosarcoma lung metastasis by repressing STAT1 and activating pulmonary cancer-associated fibroblasts. *Theranostics*. 2021;11(3):1473–1492. doi:10.7150/thno.51245
27. Deng X, Yi X, Deng J, et al. ROCK2 promotes osteosarcoma growth and metastasis by modifying PFKFB3 ubiquitination and degradation. *Exp Cell Res*. 2019;385(2):111689. doi:10.1016/j.yexcr.2019.111689
28. Wang J, Gong J, Wei Z. Strategies for liposome drug delivery systems to improve tumor treatment efficacy. *Aaps Pharmscitech*. 2021;23(1):27. doi:10.1208/s12249-021-02179-4
29. Bhattacharya S, Saindane D, Prajapati BG. Liposomal drug delivery and its potential impact on cancer research. *Anti-Cancer Agent Me*. 2022;22(15):2671–2683. doi:10.2174/1871520622666220418141640
30. Gao C, Zhang L, Tang Z, Fang Z, Ye X, Yu W. Preparation, characterization, and anti-colon cancer activity of oridonin-loaded long-circulating liposomes. *Pharm Dev Technol*. 2021;26(10):1073–1078. doi:10.1080/10837450.2021.1982966
31. Sindhwani S, Syed AM, Ngai J, et al. The entry of nanoparticles into solid tumors. *Nat Mater*. 2020;19(5):566–575. doi:10.1038/s41563-019-0566-2
32. Geng X, Gao D, Hu D, et a. Challenging paradigms in tumor drug delivery. *Nat Mater*. 2020;19(5):477. doi:10.1038/s41563-020-0676-x
33. Nunes SS, Miranda S, de Oliveira SJ, et al. pH-responsive and folate-coated liposomes encapsulating irinotecan as an alternative to improve efficacy of colorectal cancer treatment. *Biomed Pharmacother*. 2021;144:112317. doi:10.1016/j.biopha.2021.112317
34. Zhang Q, Wang J, Zhang H, et al. The anticancer efficacy of paclitaxel liposomes modified with low-toxicity hydrophobic cell-penetrating peptides in breast cancer: an in vitro and in vivo evaluation. *Rsc Adv*. 2018;8(43):24084–24093. doi:10.1039/c8ra03607a
35. Gangopadhyay S, Nikam RR, Gore KR. Folate receptor-mediated siRNA delivery: recent developments and future directions for RNAi therapeutics. *Nucleic Acid Ther*. 2021;31(4):245–270. doi:10.1089/nat.2020.0882
36. Kumar P, Huo P, Liu B. Formulation strategies for folate-targeted liposomes and their biomedical applications. *Pharmaceutics*. 2019;11(8):381. doi:10.3390/pharmaceutics11080381
37. Mengie AT, Tilahun MZ, Behaile TA, Bogale KA, Chekol AE. Role of JAK2/STAT3 signaling pathway in the tumorigenesis, chemotherapy resistance, and treatment of solid tumors: a systemic review. *J Inflamm Res*. 2022;15:1349–1364. doi:10.2147/JIR.S353489
38. Jin Y, Kang Y, Wang M, et al. Targeting polarized phenotype of microglia via IL6/JAK2/STAT3 signaling to reduce NSCLC brain metastasis. *Signal Transduct Tar*. 2022;7(1):52. doi:10.1038/s41392-022-00872-9
39. Park SY, Lee CJ, Choi JH, et al. The JAK2/STAT3/CCND2 Axis promotes colorectal Cancer stem cell persistence and radioresistance. *J Exp Clin Canc Res*. 2019;38(1):399. doi:10.1186/s13046-019-1405-7

40. De Luca A, Bellavia D, Raimondi L, et al. Multiple effects of resveratrol on osteosarcoma cell lines. *Pharmaceuticals-Base*. 2022;15(3). doi:10.3390/ph15030342
41. Wang G, Sun M, Jiang Y, et al. Anlotinib, a novel small molecular tyrosine kinase inhibitor, suppresses growth and metastasis via dual blockade of VEGFR2 and MET in osteosarcoma. *Int J Cancer*. 2019;145(4):979–993. doi:10.1002/ijc.32180
42. Hu XK, Rao SS, Tan YJ, et al. Fructose-coated Angstrom silver inhibits osteosarcoma growth and metastasis via promoting ROS-dependent apoptosis through the alteration of glucose metabolism by inhibiting PDK. *Theranostics*. 2020;10(17):7710–7729. doi:10.7150/thno.45858
43. Soares L, Lima A, Melo AS, Almeida TC, de Medeiros TL, Da SG. Additive effects of resveratrol and doxorubicin on bladder cancer cells. *Anticancer Drugs*. 2022;33(1):e389–e397. doi:10.1097/CAD.0000000000001218
44. Yang MD, Sun Y, Zhou WJ, et al. Resveratrol enhances inhibition effects of cisplatin on cell migration and invasion and tumor growth in breast cancer MDA-MB-231 cell models in vivo and in vitro. *Molecules*. 2021;26(8). doi:10.3390/molecules26082204
45. Mirzaei S, Gholami MH, Zabolian A, et al. Resveratrol augments doxorubicin and cisplatin chemotherapy: a novel therapeutic strategy. *Curr Mol Pharmacol*. 2022. doi:10.2174/1874467215666220415131344